Comparing the Performance of mScarlet-I, mRuby3, and mCherry as FRET Acceptors for mNeonGreen

Tyler W. McCullock[1], David M. MacLean[1], and Paul J. Kammermeier[1*]

[1]Department of Pharmacology and Physiology, University of Rochester Medical Center, Rochester, New York, United States of America.

* Corresponding author

Email: paul_kammermeier@urmc.rochester.edu (PJK)

Abstract

Förster Resonance Energy Transfer (FRET) has become an immensely powerful tool to profile intra- and inter-molecular interactions. Through fusion of genetically encoded fluorescent proteins (FPs) researchers have been able to detect protein oligomerization, receptor activation, and protein translocation among other biophysical phenomena. Recently, two bright monomeric red fluorescent proteins, mRuby3 and mScarlet-I, have been developed. These proteins offer much improved physical properties compared to previous generations of monomeric red FPs that should help facilitate more general adoption of Green/Red FRET. Here we assess the ability of these two proteins, along with mCherry, to act as a FRET acceptor for the bright, monomeric, green-yellow FP mNeonGreen using intensiometric FRET and 2-photon Fluorescent Lifetime Imaging Microscopy (FLIM) FRET techniques. We first determined that mNeonGreen was a stable donor for 2-photon FLIM experiments under a variety of imaging conditions. We then tested the red FP's ability to act as FRET acceptors using mNeonGreen-Red FP tandem construct. With these constructs we found that mScarlet-I and mCherry are able to efficiently FRET with mNeonGreen in spectroscopic and FLIM FRET. In contrast, mNeonGreen and mRuby3 FRET with a much lower efficiency than predicted in these same assays. We explore possible explanations for this poor performance but are unable to definitively determine the cause, all though protein maturation seems to play a role. Overall, we find that mNeonGreen is an excellent FRET donor, and both mCherry and mScarlet-I, but not mRuby3, act as practical FRET acceptors, with mScarlet-I out performing mCherry due it's higher brightness.

Introduction

42 Genetically encoded Fluorescent Proteins (FPs) have advanced basic and translational
43 biology immensely. Starting with the cloning of the *Aequorea victoria* green FP[1], a
44 massive and continual effort to expand the number of available FPs with a different
45 physical and spectral properties began. Currently, there is an enormous variety of FPs
46 at all parts of the visible spectrum, and even some parts of the ultraviolet and infrared
47 spectrums. These new proteins were either cloned from other organisms[2-4], or
48 developed through evolution of already identified FPs[4-11]. This ever expanding
49 catalog of FPs has been reviewed by others[12-14], and new efforts and archives have
50 been created to organize this information, such as the FPbase database[15].
51 As the catalogue of FPs has expanded, so have the potential uses. Of particular
52 note is the use of FPs as biosensors which can measure signaling events, cell
53 metabolites, pH, voltage and more[16]. Many of these biosensors employ Förster
54 Resonance Energy Transfer (FRET) as part of their reporting mechanism, producing a
55 change in acceptor emission upon donor excitation when the quantity of interest
56 changes. FRET is also orientation and distance dependent[17], meaning that the
57 magnitude of energy transfer (described as the FRET efficiency) can be used to study
58 either the steady state or dynamic changes in protein interactions. Much of the work
59 utilizing FPs for FRET has been done using Cyan/Yellow FP pairs due to their
60 brightness, but these proteins suffer from large overlaps in their emission spectra
61 making interpretation of results unnecessarily challenging, among other complicating
62 factors. Green/Red FP pairs offer greater separation of their emission spectra while
63 maintaining the high degree of spectral overlap between donor emission and acceptor
64 absorption that allows for efficient energy transfer. Green/Red FPs also offer greater
65 Förster radii than most Cyan/Yellow protein pairs, enabling FRET over longer distances.
66 Being able to detect FRET over larger distances often leads to greater dynamic range

67 and sensitivity. Additionally, cellular toxicity to blue light has been well documented in a
68 variety of systems[18-22], emphasizing the need for better green and red shifted FRET
69 pairs. Historically, Green/Red FRET has been limited by unfavorable fluorescent
70 properties of the red protein[23-26], but several recently developed monomeric red
71 fluorescent proteins are reported to have improved absorption, brightness, and stability
72 indicating they may act as high quality FRET acceptors for green FPs.
73 It is the aim of this study to characterize these recently released red FPs as
74 FRET acceptors in hopes of helping aid a more general adoption of Green/Red FRET.
75 Here, we investigate the ability of next generation red FPs, mRuby3 and mScarlet-I as
76 well as mCherry to act as a FRET acceptor for the green-yellow FP donor
77 mNeonGreen. mRuby3[10] is the newest iteration of the Ruby series of red FPs[8, 9]
78 originally developed from eqFP611[3]. The mScarlet series of red FPs[11] was
79 developed from a synthetic gene template based off several naturally occurring red FPs.
80 Three monomeric red FPs were evolved from this strategy, the bright variant mScarlet,
81 the fast maturing variant mScarlet-I, and the fast lifetime variant mScarlet-H. For this
82 study, we use mScarlet-I due to its fast maturation time, as slower maturation is less
83 ideal for fusion proteins studies. mCherry[6], a commonly used monomeric red FP
84 developed from DsRed[2], is included in this study to act as a standard. For the donor
85 molecule, we chose mNeonGreen[4], an incredibly bright and stable green-yellow FP
86 derived from the monomerization of the tetrameric yellow fluorescent protein LanYFP[4].
87

88 # Materials and Methods

89 ## Cell culture and transfection

90 HEK293A cells (ATCC; Manassas, VA) were maintained in Dulbecco's Modified Eagle
91 Medium (DMEM) supplemented with 1X GlutaMAX™, 100 units/mL penicillium, 100
92 µg/mL streptomycin (ThermoFisher Scientific; Waltham, MA), and 10% heat-inactivated
93 fetal bovine serum (Atlas Biologicals; Fort Collins, CO). To induce expression of
94 fluorescent proteins, cells were transiently transfected using polyethyenimine (PEI)
95 transfection. For all transfections the indicated amounts of DNA and PEI where mixed
96 together in DMEM containing no supplements for 30 minutes before addition to cells at
97 the indicated time point. For FLIM experiments, cells were plated on number 1 cover
98 slips (Warner Instruments; Hamden, CT) in 12-well plates (Nest Scientific USA;
99 Rahway, NJ) 48 hours prior to experiments. Cells were then transfected 24 before
100 experiments began using 0.6 µg of cDNA for the indicated construct and 1.6 µg of PEI
101 in 1 mL of media. For confocal experiments, cells were plated in 35 mm plastic culture
102 dishes (Corning; Corning, NY) 48-72 hours prior to experiments, followed by
103 transfection with 1 µg of cDNA using 2.4 µg of PEI in 2 mL of media 24-36 hours before
104 imaging began. For spectral FRET and immunoblotting experiments, cells were plated
105 in 10 cm plastic culture dishes and allowed to grow to 70% confluency. Cells were then
106 transfected with 4 µg of cDNA using 7.8 µg of PEI 24 hours before experiments started.
107

108 Plasmids and cloning

109 All constructs used in this manuscript are derived from the pKanCMV-mClover3-
110 mRuby3 plasmid (Plasmid #74252) available on Addgene.org (Addgene; Watertown,
111 MA). NG-Ruby3 was created by removing mClover3 and all but the last 5 amino acids
112 of the linker from pKanCMV-mClover3-mRuby3 by inverse PCR, and the full
113 mNeonGreen coding sequence was inserted in its place using In-Fusion cloning

114 (Takara Bio; Mountain View, CA). NG-Scarlet and NG-Cherry were created by deleting
115 mRuby3 from NG-Ruby3 by inverse PCR and insertion of either mScarlet-I or mCherry
116 using In-Fusion cloning (Takara Bio). NG-Stop was created using the same inverse
117 PCR product as NG-Scarlet and NG-Cherry via blunt end ligation using NEBs KLD Mix
118 (New England Biolabs; Ipswich, MA). The mNeonGreen gene was obtained from the
119 pmNeonGreen-NT plasmid (Allele Biotehcnology; San Diego, CA), the mScarlet-I gene
120 was obtained from the Lck-mScarlet-I plasmid (Addgene, plasmid #98821), and the
121 mCherry gene was obtained from the pmCherry-N1 plasmid (Takara Bio). Reaction
122 products were transformed, screened, and amplified in XL10-Gold Ultracompetent *E.*
123 *coli* cells (Agilent Technologies; Santa Clara, CA). Plasmid were isolated using an
124 E.Z.N.A Plasmid MiniPrep Kit (Omega Bio-teck; Norcross, GA) or a ZymoPure II
125 Plasmid Midiprep Kit (Zymo Research; Irvine, CA) per manufactures recommendations.
126 All constructs were verified by sanger sequencing (Eurofins Genomics; Louisville, KY)
127 and stored at a concentration of 1μg/μL in a -20°C freezer. All plasmids and constructs
128 generated for this manuscript are available upon request.
129

130 Spectral FRET

131 For spectral FRET experiments, cells were used 24-36 hours post transfection. A single
132 10 cm dish of cells expressing the construct of interest were washed with imaging buffer
133 (136 mM NaCl, 560 μM $MgCl_2$, 4.7 mM KCl, 1 mM Na_2HPO_4, 1.2 mM $CaCl_2$, 10 mM
134 HEPES, 5.5 mM Glucose) several times and pelleted. Cell pellets were then
135 resuspended in 500 μL of imaging buffer and transferred to disposable acrylate cuvettes
136 (Spectrocell Inc; Oreland, PA). Emission scans were collected from 490-750 nm using a
137 470 nm excitation wavelength using a Cary Eclipse Fluorescence Spectrophotometer

138 (Agilent Technologies). Cell were resuspended by vigorous pipetting immediately prior
139 to scans. Data was collected in the Cary Eclipse Scan Application software package
140 (Agilent Technologies) and exported to Microsoft Excel (Microsoft Corporation) for
141 analysis. To estimate FRET efficiency from emission scans, linear unmixing was
142 performed in Igor Pro (WaveMetrics Inc; Lake Oswego OR) using donor only and
143 acceptor only emission scans to determine the contributions of donor and acceptor. Due
144 to the high level of consistency between the NG-Stop and reported spectrum for purified
145 mNeonGreen (S2 Fig), the purified mNeonGreen spectrum was used as the donor only
146 scan for linear unmixing. For each of the acceptors, custom acceptor only scans were
147 created based on experimentally collected data and their reported purified spectrum (as
148 discussed in S2 Fig). All raw scans used for spectral FRET are available in S2 Fig.
149 Once the contributing weight of donor and acceptor was determined, FRET efficiency
150 was estimated using the following equation[27]:

151 $$E = \frac{W_A}{\left(\frac{QY_A}{QY_D}\right)W_D + W_A} x\, 100\% \quad (1)$$

152 where E is the FRET efficiency, W_A and W_D are the component weights of the donor
153 only and acceptor only emissions calculated through linear unmixing, and QY_A and QY_D
154 is the quantum yield of the acceptor and donor respectively.
155

156 Fluorescent lifetime imaging microscopy (FLIM)

157 For FLIM experiments, cells were used 1-day post transfection unless otherwise noted.
158 30 minutes before experiments begin, media was exchanged for imaging buffer and
159 allowed to come to room temperature. Coverslips were transferred to a custom-built
160 chamber and mounted onto the stage of an Olympus FluoView 1000-MP Multiphoton

161 and Scanning Confocal Microscope (Olympus; Tokyo, Japan). Excitation of samples
162 was achieved using a Mai Tai Ti:Sapphire Femtosecond Pulse Laser (Spectra-Physics;
163 Santa Clara, CA) tuned to 950 nm. Fluorescent decays were collected using a XLPlan N
164 25x (NA 1.05) water immersion objective (Olympus) at 256x256 resolution and a pixel
165 dwell time of 20 μsec. The data was passed by the microscope to the FLIM set up,
166 consisting of two H7422P Hamamatsu detectors (Hamamatsu; Hamamatsu City, Japan)
167 and a time-correlated single photon counting card (Becker and Hickl; Berlin, Germany).
168 To separate donor and acceptor emission, a BrightLine FF552-Bi02-25x36 dichroic
169 (Semrock; Rochester, NY) was used. Emission light to the donor detector was further
170 filtered with a BrightLine FF01-510/42-25 filter and emission to the acceptor detector
171 was filtered with a BrightLine FF01-609/54-25 filter (Semrock). The microscope was
172 controlled with the FV10-ASW software package (Olympus) and the FLIM system was
173 controlled via the VistaVision by ISS software package (ISS Inc; Champaign, IL).
174 Analysis of single cell lifetime decays was performed with VistaVision by ISS and
175 subsequent lifetimes were analyzed in Microsoft Excel (Microsoft Corporation;
176 Redmond, WA). Briefly, cells were isolated into individual regions of interest (ROIs), and
177 the decay data for each pixel in the region above threshold were summed to create a
178 cell fluorescence decay curve. These decay curves were then fit and lifetimes were
179 extracted using non-linear regression in tail-fitting mode. Almost all decay curves were
180 well described by a single exponential fit (as determined by Chi-squared analysis as
181 well as by eye). Lifetimes were extracted from these fits and used to calculate FRET
182 efficiency using the following equation[28]:
183
184 $$E = 1 - (\tau_{DA}/\tau_D) \quad (2)$$
185

186 Where E is the FRET efficiency, τ_{DA} is the lifetime of the donor in the presence of
187 acceptor, and τ_D is the lifetime of the donor only species (in this case, the average
188 lifetime of NG-Stop). For experiments where acceptor photobleaching was preformed,
189 cells were bleached by scanning with a 559 nm laser at 100% power for 15 minutes
190 under the same parameters that the lifetime data was collected.
191

192 Confocal microscopy

193 For confocal microscopy experiments, cells were used 1-day post transfection. 30
194 minutes before experiments began, media was exchanged for imaging buffer and
195 allowed to come to room temperature. Images were then collected on the same
196 microscope as the FLIM data utilizing a SIM scanner and 488 nm and 559 nm
197 conventional laser lines. Widefield confocal images were collected through a
198 XLUMPlanFl 20X (NA 0.95) water immersion objective (Olympus) at a resolution of
199 2048x2048. The sample was excited, and emission collected in each channel
200 individually to prevent blead through. Green emission was collected through a 505-540
201 nm filter and red emission was collected through a 575-675 nm filter. All imaging
202 parameters were kept consistent across experiments to facilitate comparisons. Data
203 was collected in FV10-ASW software package (Olympus) and exported to the Fiji
204 software package[29] for analysis as described in the main text and S2 Fig using the
205 Coloc2 plugin.
206

207 Immunoblotting

208 Samples for immunoblotting were harvested 24 hours after transfection. Cells were
209 removed from their culture dish and washed twice with calcium and magnesium free

210 DPBS (Corning). Following cell lyses in the presence of protease inhbitors, protein
211 concentrations were evaluated using a Pierce™ BCA Protein Assay Kit (ThermoFisher
212 Scientific) and 10 µg of total protein was loaded into a 16% SDS-PAGE gel. After
213 electrophoresis, proteins were transferred to a 0.2 µm nitrocellulose membrane
214 (BioRad; Hercules, CA). Presence of the mNeonGreen protein was probed using a
215 monoclonal mNeonGreen antibody [32F6] (Chromotek; Planegg-Martinsried, Germany)
216 at a 1:1000 dilution and visualized using a DyLight 680 secondary antibody
217 (ThermoFisher Scientific) at a 1:1000 dilution using an Odyssey 3 Imaging System (Li-
218 cor Biosciences; Lincoln, NE).
219

220 Statistics

221 To avoid assumptions regarding the data distributions, all statistical significance in this
222 manuscript was determined using a permutation test implemented through a custom
223 Python script utilizing the MLxtend library[30] using the approximation method with
224 1,000,000 permutations. For instances where there was less than 10 data points total
225 between the two data sets being compared, an exact method was used.
226

227 Results

228 Physical properties and spectrum of proteins in this study

229 For this study, we utilized the monomeric, yellow-green fluorescent protein
230 mNeonGreen to test the ability of two new red fluorescent proteins, mRuby3 and
231 mScarlet-I, as well as mCherry to act as FRET acceptors. The fluorescent and physical
232 properties of these proteins are listed in Table 1. mNeonGreen is one of the brightest
233 fluorescent proteins to date with a high quantum yield and extinction coefficient making

234 it's signals easy to observe. In addition, mNeonGreen is also highly photostable[4],
235 making it an ideal FRET donor. Both mRuby3 and mScarlet-I have high extinction
236 coefficients, poising them to be excellent FRET acceptors. In comparison to mCherry,
237 these proteins also offer substantially higher quantum yield, indicating that it will be
238 easier to detect energy transfer events using the emission of one of these two proteins.
239 The absorbance and emission spectrum of mNeonGreen is overlaid with the spectrum
240 of mRuby3, mScarlet-I and mCherry in Fig 1A-C. For each red fluorescent protein, the
241 overlap integral ($J(\lambda)$) and Förster radius (R_0) values with mNeonGreen are listed in
242 Table 1. Based on these photophysical properties, all three red FPs are expected to
243 FRET with mNeonGreen. Assuming identical positioning between donor and acceptor,
244 mRuby3 is expected to produce the highest FRET efficiency and mCherry the lowest
245 FRET efficiency with mNeonGreen.

246

247 **Table 1. Properties of the fluorescent proteins used in this study**

Protein	Ref	λ_{ex} max (nm)	λ_{em} max (nm)	EC ($M^{-1}cm^{-1}$)	QY	pKa	Maturation (min)	$J(\lambda)$ ($x10^{15}$ $M^{-1}cm^{-1}nm^4$)	R_0 (Å)
Donor									
mNeonGreen	4	506	517	116,000	0.8	5.7	10	-	-
Acceptors									
mRuby3	10	558	592	128,000	0.45	4.8	136.5	4.65	64
mScarlet-I	11	569	593	104,000	0.54	5.4	36	3.60	61
mCherry	6	587	610	72,000	0.22	4.5	15	2.28	57

248 λ_{ex} max = emission maximum, λ_{em} = emission maximum, EC = extinction coefficient, QY = quantum yield, $J(\lambda)$ =
249 overlap integral, R_0 = Förster Radius. $J(\lambda)$ and R_0 are calculated with mNeonGreen as the donor, an orientation factor
250 of 0.6667, and a refractive index of 1.33. Values were obtained from the references listed under the Ref column.

251

252 **Fig 1. Spectrum of mNeonGreen, mRuby3, mScarlet-I and mCherry.** Absorbance (dashed lines) and emission
253 spectrum (solid lines) of purified mNeonGreen (green lines) overlaid with the spectrum of purified mRuby3 **(A)**,
254 mScarlet-I **(B)**, and mCherry **(C)**. Spectrum were obtained from the reference indicated in Table 1.

mNeonGreen-RFP tandem constructs reveal poor performance of mRuby3

To test the ability of the red FPs to act as FRET acceptors, we constructed tandem FP constructs consisting of the full coding sequence of mNeonGreen followed by a short amino acid linker (SKGEE) and then the full coding sequence of the red FP (Fig 2A). Although a 5 amino acid linker is relatively short, inclusion of the full mNeonGreen c-terminus (which appears unstructured or absent in the mNeonGreen structure[31]) creates an effective linker of 17 amino acids. A mNeonGreen-Stop construct was also created, which contains the full coding sequence of mNeonGreen, the 5 amino acid linker, and then a stop codon to act as a donor only control construct. To determine if mNeonGreen will FRET with the red FPs in these constructs, we transiently transfected each construct into HEK293 cells and measured the acceptor FP emission upon excitation with a wavelength that will only excite the donor. When cells expressing the NG-Stop constructs are excited with 470 nm light, a spectrum comparable to what has been reported for purified mNeonGreen was obtained (Fig 2B, S1 Fig in the Supplemental Information). When the NG-red FP tandem constructs are assayed, a second peak emerges corresponding to the red FP. Example spectrum for the NG-Ruby3, NG-Scarlet, and NG-Cherry constructs are shown in Fig 2C, 2D, and 2E respectively in pink, along with calculated donor (green) and acceptor components (red) determined through linear unmixing, as well as the fit (black dashed line) resulting from the addition calculated donor and acceptor components. Note that in all cases, the unmixing fit faithfully reproduced the raw data traces. Using the donor and acceptor components, the FRET efficiency of each construct can be estimated using Eq. 1 (Fig 2F, with the raw traces available in S1 Fig). Over three independent transfections for

each construct, the NG-Scarlet and NG-Cherry construct presented a FRET efficiency of 29 ± 0.5% and 22 ± 0.8% respectively. Surprisingly, the NG-Ruby3 construct presented an estimated FRET efficiency of 16 ± 0.1%. This poor performance in comparison to NG-Scarlet or NG-Cherry was highly unexpected considering the physical and spectral properties reported for mRuby3[10], which predicted it would be the best FRET acceptor of the three red FPs for mNeonGreen.

Fig 2. Spectral FRET of each mNeonGreen-Red FP tandem constructs. (A) Cartoon schematic of the mNeonGreen-Red FP tandem constructs used for FRET experiments. **(B)** Average emission scan of cells expressing NG-Stop (black) when excited at 470 nm overlaid with the reported spectrum for purified mNeonGreen in green (n = 3 independent transfections). Example raw emission spectrum (pink) of tandem **(C)** NG-Ruby3, **(D)** NG-Scarlet, and **(E)** NG-Cherry when excited at 470 nm. The dashed black line shows the sum of donor (green) and acceptor (red) components calculated by linear unmixing. **(F)** FRET efficiencies calculated from the spectrum for each construct (n=3). *** = P < 0.0005 between the indicated conditions.

mNeonGreen is a suitable donor for two-photon FLIM

To confirm our spectral FRET findings, we turned to the more precise method of 2-Photon Fluorescent Lifetime Imaging (FLIM). First sought to determine if mNeonGreen was a suitable donor for 2-Photon FLIM experiments. A well-behaved FRET donor would be easily excited by the 2-photon laser, be stable under a variety of 2-photon laser powers, and display a stable, mono-exponential lifetime[32]. To our knowledge, there is only one report of mNeonGreen's performance using two-photon illumination[33]. This study demonstrated that blue shifted fluorescent proteins tend to perform better under 2-photon excitation than more yellow shifted fluorescent proteins but did not preclude mNeonGreen's use from two-photon based studies. Using 950 nm light and the NG-Stop construct, we assayed mNeonGreen's performance in 2-photon FLIM over various conditions using Time Correlated Single Photon Counting. Over a

305 variety of laser powers, mNeonGreen produced a stable lifetime of 3.05 ± 0.01 ns over
306 50 frames of acquisition (Fig 3A). This lifetime was stable for up to 300 frames of
307 acquisition for all but the highest laser power tested, 25 W/cm^2 in which the lifetime
308 linearly decayed to 87 ± 4.5% of its initial value after 300 frames (Fig 3B). In contrast,
309 significant photobleaching was observed for laser powers above 15 W/cm^2 (Fig 3C) with
310 20 W/cm^2 and 25 W/cm^2 bleaching approximately 48 ± 14% and 94 ± 3% of the sample
311 intensity respectively after 300 frames. Example decay traces of a single cell collected
312 in consecutive 50 frame intervals are shown at 15 W/cm^2 (Fig 3D) and 25 W/cm^2 (Fig
313 3E). Normalizing the decay traces to the peak intensity for the 25 W/cm^2 example
314 demonstrates the reduction in lifetime and the decay in data quality over the course of
315 acquisition at this power (Fig 2F). Given these data, we conclude that mNeonGreen is a
316 suitable donor for two-photon FLIM experiments when the lifetime is acquired at a laser
317 power of 15 W/cm^2 or less. For all further FLIM experiments, data was collected at laser
318 powers between 5-10 W/cm^2 for 100-150 frames depending on the brightness of the
319 cell.
320
321 **Fig 3. mNeonGreen performs well under various laser powers for two-photon time domain FLIM acquisitions.**
322 **(A)** Lifetime data collected from individual HEK293 cells expressing cytosolic mNeonGreen at various laser powers
323 up to 25 W/cm^2 after 50 frames. Black bars indicate the average ± 95% confidence interval. **(B)** Lifetime and **(C)**
324 intensity of samples taken over 300 frames at various laser powers. * = P < 0.05, ** = P< 0.005, and *** = P < 0.0005
325 compared to the frame matched 5W/cm^2 dataset. N for each sample is as follows 5W/cm^2: 11 cells, 10W/cm^2: 10
326 cells, 15W/cm^2: 14 cells, 20W/cm^2: 9 cells, 25W/cm^2: 11 cells. **(D)** Example lifetime decay curves obtained at 15
327 W/cm^2 over 300 frames. **(E)** Example lifetime decay and normalized decays **(F)** obtained at 25 W/cm^2 over 300
328 frames.

329 FLIM-FRET measurements confirm poor performance of
330 mRuby3

With FLIM, FRET is detected as a reduction of the donor's lifetime when in the presence of the acceptor[28]. This technique has the advantage of determining the FRET state between mNeonGreen and the red FP independent of the red FPs emission, allowing us to determine the FRET efficiency for each construct without having to account for the differences between each red FPs. Over the course of several independent transfections, the mNG-Stop construct produced a donor only lifetime of 3.05 ± 0.02 ns (Fig 4A). When mScarlet-I or mCherry are present in the tandems, mNeonGreen's lifetime is reduced to 2.22 ± 0.06 ns and 2.23 ± 0.03 ns respectively (Fig 4A). This results in a FRET efficiency of the NG-Scarlet construct of 27 ± 2% and an efficiency of 27 ± 1% for the NG-Cherry construct (Fig 4B). Assay of the NG-Ruby3 construct shows even worse performance of mRuby3 than what was estimated with spectral FRET (Fig 2F). The average lifetime of the NG-Ruby3 construct was 2.92 ± 0.03 ns (Fig 4A) resulting in a FRET efficiency of only 4 ± 0.9% (Fig 4B). Indeed, 35 cells across 3 independent transfections (over half of all cells sampled) exhibited lifetimes within the range of what was collected for the NG-Stop construct, whereas no cells expressing NG-Scarlet or NG-Cherry had lifetimes within that range (Fig 4A). Example decay traces representative of the average for each construct are shown in Fig 4C and example lifetime maps of HEK293 cells expressing each construct are shown in Fig 4D.

Fig 4. Lifetime of mNeonGreen-Red FP tandem constructs. (A) The lifetime of mNeonGreen in individual cells expressing a mNeonGreen-Red Protein tandem fusion construct. Black bars indicate the average ± 95% confidence interval. **(B)** FRET efficiency calculations for each tandem construct. *** = $P < 0.005$ compared to NG-Stop and # indicates $P < 0.0005$ compared to NG-Stop and $P < 0.0005$ compared to NG-Ruby3. NG-Scarlet and NG-Cherry are not statistically different ($P=0.75$) **(C)** Example decay curves for each tandem representative of the average lifetime of all cells for each construct. **(D)** Example lifetime heat maps for a single frame for each construct. N for each construct is as follows NG-Stop: 68 cells, NG-Ruby3: 63 cells, NG-Scarlet: 64 cells, and NG-Cherry: 64 cells.

357 ***Confocal imaging demonstrates lower than expected red***

358 ***fluorescence for mNeonGreen-mRuby3 construct***

359 To further investigate the poor performance of mRuby3 as a FRET acceptor, we turned
360 to confocal microscopy to analyze the behavior each tandem construct. The presence of
361 mNeonGreen and the red FPs were independently surveyed via sequential excitation
362 with a 488 nm and 559 nm lasers, with the emissions of each channel being collected
363 separately to prevent bleed through. Example wide field images of cells expressing
364 each construct are shown in Fig 5A. Qualitatively, it can be seen in the merged image of
365 the green and red channels that the cells expressing the NG-Ruby3 construct had
366 widely varying intensities of green and red fluorescence. Interestingly, cells were
367 regularly observed that seem to contain high levels of mNeonGreen and low levels of
368 mRuby3 or vice versa, alongside cells that appeared to contain both proteins. This
369 heterogeneity was also noted in with the NG-Scarlet and NG-Cherry constructs, but with
370 much less frequency (Fig 5A). This result was quite surprising given the constructs were
371 designed to express mNeonGreen and the red FP stoichiometrically and in tandem.
372 Theoretically, we would expect expression of such tandem constructs to result in a fixed
373 ratio of green to red intensity where the red intensity varies depending on the brightness
374 of the red FP and the extent of FRET. To test this prediction and quantify the
375 heterogeneity for each construct we examined regions of interest (ROI) containing a
376 single cell, extracted the green and red intensities for that cell following background
377 subtraction, and plotted the resulting intensities at the pixel level. The resulting green-
378 red intensity plots for each cell were then fit with a linear regression. An example of this
379 workflow is diagramed in S2 Fig. While the absolute value of this slope will be different
380 for each fluorophore pair and for different imaging conditions, the changes in this slope

381 from cell to cell under the same imaging conditions will report the heterogeneity of each
382 construct. As expected of a tandem construct and based on qualitative assessments of
383 images (Fig 5A), histograms of the slopes for individual cell expressing the NG-Cherry
384 and NG-Scarlet constructs revealed a reasonable distribution and narrow spread of
385 slopes (Fig 5C,D). This indicates the majority of cells expressing these constructs
386 contain a fixed ratio of mNeonGreen to red FP. In contrast, the histogram of slopes from
387 cells expressing NG-Ruby3 were not as evenly distributed (Fig 5B). Indeed, the majority
388 of cells expressing this construct have a slope close to 0, suggesting that these cells
389 contain measurable mNeonGreen levels but low levels of fluorescent mRuby3.
390 Interestingly, this lack of abundant red fluorescence does not stem from a lack of
391 mRuby3 protein as western blotting of cells transfected with NG-Ruby3 produce a
392 similar banding pattern as those transfected with NG-Scarlet and NG-Cherry (S3 Fig).
393 Importantly, in NG-Ruby3 transfected cells there is no smaller monomer sized band,
394 indicating our tandem constructs are generally intact and ruling out the possibility of
395 mNeonGreen produced without mRuby3. Taken together, these data provide a
396 mechanistic explanation for our FLIM data in which all cells expressing the NG-Scarlet
397 and NG-Cherry constructs exhibited robust FRET, whereas a large majority of NG-
398 Ruby3 constructs did not. Further, they suggest that the poor performance of NG-Ruby3
399 may be due to poor maturation of the acceptor compared to NG-Scarlet and even NG-
400 Cherry.

401

402 **Fig 5. Confocal microscopy of the tandem constructs. (A)** Example images of NG-Red FP constructs when
403 directly excited by 499 nm or 559 nm lasers. Histograms of the slopes of the red/green intensity correlations for
404 individual cells expressing **(B)** NG-Ruby3 (n=1077 cells), **(C)** NG-Scarlet (n = 1745 cells), and **(D)** NG-Cherry (n=
405 1557 cells).

Expressing mNeonGreen-Ruby3 for longer periods of time improves its performance

To determine if the poor performance of mRuby3 as a FRET acceptor is due at least in part due to inefficient maturation, we performed FLIM experiments for up to five days following transient transfection with the NG-Ruby3 construct. As seen in Fig 6A, the average lifetime of mNeonGreen in the NG-Ruby3 construct decreases from 2.92 ± 0.03 ns 1-day post transfection (DPT) to 2.41 ± 0.09 ns 5 DPT. This results in a change in average FRET efficiency of 4 ± 0.9% 1 DPT to an efficiency of 21 ± 3.0% efficiency 5 DPT transfection (Fig 6B). Example lifetime maps of individual cells expressing NG-Ruby3 2-5 DPT are shown in Fig 6C, with the example lifetime map for 1 DPT shown in Fig 3D. Example fluorescent decay traces for each DPT are available in S4 Fig. As time progressed, the number of cells exhibiting lifetimes within the range of the NG-Stop also decreased. However, even 5 DPT cells could still be observed that exhibited donor only like lifetimes. This indicates that although inefficient maturation in mammalian cells may be part of the reason mRuby3 performs poorly in previous experiments, it is likely not the only contributing factor. To ensure that the changes observed over time for the NG-Ruby3 construct were due to changes occurring to the mRuby3 protein, and not mNeonGreen, mNeonGreen lifetimes of the NG-Ruby3 constructs were determined before and after acceptor photobleaching on 5 DPT (Fig 6D). Regardless of the lifetime each cell exhibited before acceptor photobleaching, all cells exhibited lifetimes similar to that of the NG-Stop construct after acceptor photobleaching. Fig 6F shows example lifetime maps of two cells expressing NG-Ruby3 5 days post transfection before and after acceptor photobleaching and example fluorescent decay traces can be found in S4 Fig. These findings demonstrate that the mNeonGreen lifetime remained stable over the

course of 5 days, indicating that the changes the NG-Ruby3 construct underwent was due to changes occurring to the mRuby3 protein.

Fig 6. FRET of NG-Ruby3 1-5 days post transfection. (A) Lifetimes of cells expressing NG-Ruby3 construct 1-5 days post transfection (DPT) with 1 DPT is replicated from Fig 3A for reference. Black bars indicated the average lifetime ± 95% confidence interval. The green shading indicates the range of lifetimes observed from the NG-Stop construct. *** = P < 0.0005 compared to 1 DPT, and # = P < 0.0005 compared to 1 DPT and P < 0.0005 compared to the day before. N for each condition is as follows, 2 DPT: 30 cells, 3 DPT: 34 cells, 4 DPT: 35 cells, and 5 DPT: 31 cells. **(B)** Average FRET efficiency of NG-Ruby3 1-5 DPT. **(C)** Example lifetime maps collected each day tested. **(D)** Lifetime data from NG-Ruby3 expressing cells 5 days post transfection before and after acceptor photobleaching (n = 15). *** = P < 0.0005 after photobleaching compared to before photobleaching. **(E)** Example lifetime maps of the same cells before and after acceptor photobleaching.

Discussion

Development and verification of bright monomeric Green/Red FP pairs will greatly increase the general adoption of Green/Red FRET. Bright fluorophores allow for easier detection and greater signal to noise ratio. Using green and red fluorophores specifically has several distinct advantages include reduced toxicity by the excitation source, greater spectral separation, larger Förster radii, and better tissue penetrance. These benefits allow for newer, more accurate and precise studies to be conducted with less confounding factors than what could be done with Cyan/Yellow FRET pairs. mNeonGreen is an ideal donor for Green/Red FRET experiments. Its yellow shifted excitation and emission spectrum allow for a high degree of overlap with red FPs while also being capable of being excited with lower energy blue light than cyan or more blue shifted green FPs. In addition, mNeonGreen is remarkably bright under single-photon illumination, making its signals easy to observe. Both mScarlet-I and mRuby3 are reported as having some of the highest extinction coefficients of any red FPs, as well as also being some of the brightest monomeric red FPs to date. These facts indicate that

456 they should make excellent FRET acceptors, making Green/Red FRET more accessible
457 to researchers. In this study, we aimed to test this prediction using a variety of optical
458 techniques.

459 We tested the ability of these two new red FPs – mRuby3 and mScarlet-I – along
460 with mCherry to act as FRET acceptors for mNeonGreen using a tandem protein
461 approach. Initially we used intensiometric spectral FRET to estimate the FRET
462 efficiency between mNeonGreen and the red FPs (Fig 2). In this assay NG-Scarlet
463 demonstrated the highest FRET efficiency, followed by NG-Cherry, and then NG-Ruby3
464 (Fig 2F). This was surprising given the reported properties of mRuby3 predicted that it
465 would be the best acceptor for mNeonGreen. Specifically, mRuby3 had the highest
466 degree of overlap between its excitation spectrum and mNeonGreen's emission
467 spectrum and it has the highest extinction coefficient of the three red FPs in this study.
468 These experiments also demonstrated the advantages of these newer proteins over
469 mCherry, as mScarlet-I produced almost 3 times the intensity of mCherry, despite only
470 a 7% difference in estimated efficiency, and mRuby3 produced almost 1.5 times the
471 intensity of mCherry, despite NG-Ruby3 exhibiting a lower FRET efficiency than NG-
472 Cherry. This reflects the difference in extinction coefficient and quantum yield between
473 these two proteins and mCherry and demonstrates how mScarlet-I is a better overall
474 acceptor that will provide more signal and greater dynamic range for green-red based
475 FRET experiments.

476 To confirm these results, we turned to a more precise technique, FLIM. FLIM has
477 the advantages of only needing to observe only the donor, there for eliminating the need
478 to correct our data for differences in the acceptors physical properties as reported by
479 others. In addition, our FLIM set up allows for assaying single cells to allow for a more
480 detailed profile of the tandem construct's behavior. After establishing mNeonGreen as a

481 suitable donor for 2-Photon FLIM experiments (Fig 3), we used this technique to
482 measure the FRET efficiency of each tandem in the study (Fig 4). We found that both
483 mScarlet-I and mCherry were able to efficiently FRET with mNeonGreen as almost to
484 the same degree, but that mRuby3 was unable to induce substantial FRET (Fig 4A-B). It
485 was somewhat surprising to see mCherry preformed just as well as mScarlet-I as a
486 FRET acceptor in our FLIM experiments, despite having a significantly lower extinction
487 coefficient. This is likely due to the relatively short linker between mNeonGreen and the
488 red FPs in this study, resulting in FPs placed in close proximity and biasing towards
489 higher FRET efficiencies. In principle, as the distance between mNeonGreen and either
490 mScarlet-I or mCherry increases, the FRET efficiency between the two will diverge such
491 that the mCherry FRET efficiency will drop off compared with mScarlet-I. To further
492 investigate mRuby3s poor performance, we employed confocal microscopy to reveal
493 great heterogeneity in the way the NG-Ruby3 tandem expresses (Fig 5A-B), with many
494 cells exhibiting either red or green fluorescence, without the other. This was in spite of
495 western blotting analysis suggesting that most cells should be expressing the full-length
496 tandem protein (S4 Fig).

497 In theory, the higher extinction coefficient and quantum yield of mRuby3 predicts
498 that it should outperform the other red FPs tested herein. Shockingly though, we found
499 the opposite result (Fig 2 and Fig 4). Even under the most ideal conditions tested (4 or 5
500 days post transfection), the NG-Ruby3 tandem still did not reach the FRET efficiencies
501 of the NG-Scarlet and NG-Cherry tandems (Fig 6). This is in contrast to a previous
502 report of a similar mNeonGreen-mRuby3 construct preforming very well, achieving
503 nearly 40% efficiency in both HEK293 and Hela cells[10]. At this point, the reasons for
504 this discrepancy is unclear, although similarities in linker length and composition,
505 transfection times, and cell types suggest it is not due to a difference between the

506 makeup of the tandem constructs used or differences in the conditions in which the
507 experiments were conducted (for what conditions were reported). In addition, we found
508 during our experiments that the emission spectrum of mRuby3 in this tandem was
509 slightly left shifted by 6 nm compared to what is reported purified mRuby3[10] (S1 Fig).
510 This finding was not reported previously and although this shift was slight, it was
511 necessary to correct for it in order to properly fit our data. The cause of this spectral shift
512 remains unclear and may simply be a result of mRuby3 having slightly different behavior
513 in cells verse in a purified system. This may also be due to the photochromic behavior
514 previously reported for mRuby3[11]. Whatever the cause, unpredictable changes in
515 spectrum are highly concerning for FRET experiments as they can result in changes in
516 fluorescence intensity that may be misinterpreted as changes in FRET state. It is
517 possible that that this behavior also influenced our spectral FRET experiments (Fig 2)
518 and could account for the disparity between the calculated FRET efficiencies for the
519 NG-Ruby3 construct in the spectral FRET vs. FLIM assays.
520 While few studies using mRuby3 have been published to date, studies utilizing its
521 predecessor, mRuby2 report generally positive results[4, 9-11, 34, 35]. Although, a
522 similar study to ours using the green FP mClover as a donor reported much lower than
523 expected efficiencies when using mRuby2 as an acceptor[36]. A commonality between
524 our study and theirs is the use of mammalian cells lines. This coupled with our
525 transfection time course data (Fig 6) suggest that poor maturation efficiency of the Ruby
526 series may play a part in mRuby3's poor performance 1-3 days post transfection. This
527 would also help explain the dysregulation in mNeonGreen and mRuby3 levels we saw
528 under confocal microscopy in cells transiently transfected with the NG-Ruby3 tandem
529 one day post transfection (Fig 5), even when the full tandem appears to be present as
530 determined by western blot (S3 Fig). Poor protein stability could also cause similar

results shown here. The NG-Scarlet and NG-Cherry constructs utilize the same protein linker as NG-Ruby3 but no cells expressing them reported lifetimes similar to those of the donor only control in the FLIM assay (Fig 4A). Additionally, western blotting of cells expressing the NG-Ruby3 construct do not show a band corresponding to free mNeonGreen (S3 Fig), but all three tandems show a band between 37 and 50kDa. This suggests that the linker is not a substrate for intracellular proteases, but some part of the red FPs may be. Consistent with this, cleavage of the original mRuby protein has been reported, although the exact cleavage site was not discovered[37]. Whether cleavage of mRuby3 plays a role in its behavior in mammalian cells remains unclear. The western blot does suggest that all of these red FPs may undergo some consistent cleavage, producing a species with a molecular weight of just under 50 kDa, but why that would affect mRuby3's performance but not mScarlet-I or mCherry's performance is still unknown. Although we cannot definitively explain the causes, we can conclude that mScarlet-I is a superior choice for Green/Red FRET, and possibly other fluorescent microscopy experiments for a variety of reasons discussed here.

Conclusion

In this study, we test the viability of mNeonGreen as a FRET donor, and mRuby3, mScarlet-I, and mCherry as FRET acceptors. We find that mNeonGreen performs well as a FRET donor in both intensiometric and 2-photon FLIM experiments. When testing the red FPs as acceptors for mNeonGreen, we found that both mScarlet-I and mCherry were readily able to FRET with mNeonGreen. These proteins preformed equally well in FLIM experiments, but mScarlet-I outperformed mCherry in the intensiometric study due to its higher quantum yield. In contrast, we find that mRuby3

performs poorly as a FRET acceptor in mammalian systems, despite it being predicted to be the best FRET acceptor of the three proteins. The reason for this poor performance remains unclear, although it is likely a combination of poor maturation efficiency and poor protein stability.

Overall, we found that mNeonGreen makes an excellent green-yellow donor, and mScarlet-I is one of the best all-around acceptors for green-red FRET experiments utilizing fluorescent proteins.

Acknowledgements

We would like to thank both David Yule and Andrew Wojtovich for helpful comments over the course of the study, as well as generous sharing of equipment.

References

1. Prasher DC, Eckenrode VK, Ward WW, Prendergast FG, Cormier MJ. Primary structure of the Aequorea victoria green-fluorescent protein. Gene. 1992;111(2):229-33. doi: https://doi.org/10.1016/0378-1119(92)90691-H.

2. Matz MV, Fradkov AF, Labas YA, Savitsky AP, Zaraisky AG, Markelov ML, et al. Fluorescent proteins from nonbioluminescent Anthozoa species. Nature biotechnology. 1999;17(10):969-73. doi: 10.1038/13657.

3. Wiedenmann J, Schenk A, Rocker C, Girod A, Spindler KD, Nienhaus GU. A far-red fluorescent protein with fast maturation and reduced oligomerization tendency from Entacmaea quadricolor (Anthozoa, Actinaria). Proc Natl Acad Sci U S A.

577 2002;99(18):11646-51. Epub 2002/08/20. doi: 10.1073/pnas.182157199. PubMed
578 PMID: 12185250; PubMed Central PMCID: PMCPMC129323.
579 4. Shaner NC, Lambert GG, Chammas A, Ni Y, Cranfill PJ, Baird MA, et al. A bright
580 monomeric green fluorescent protein derived from Branchiostoma lanceolatum. Nature
581 methods. 2013;10(5):407-9. Epub 2013/03/26. doi: 10.1038/nmeth.2413. PubMed
582 PMID: 23524392; PubMed Central PMCID: PMCPMC3811051.
583 5. Aliye N, Fabbretti A, Lupidi G, Tsekoa T, Spurio R. Engineering color variants of
584 green fluorescent protein (GFP) for thermostability, pH-sensitivity, and improved folding
585 kinetics. Applied microbiology and biotechnology. 2015;99(3):1205-16. Epub
586 2014/08/13. doi: 10.1007/s00253-014-5975-1. PubMed PMID: 25112226.
587 6. Shaner NC, Campbell RE, Steinbach PA, Giepmans BN, Palmer AE, Tsien RY.
588 Improved monomeric red, orange and yellow fluorescent proteins derived from
589 Discosoma sp. red fluorescent protein. Nature biotechnology. 2004;22(12):1567-72.
590 Epub 2004/11/24. doi: 10.1038/nbt1037. PubMed PMID: 15558047.
591 7. Bayle V, Nussaume L, Bhat RA. Combination of novel green fluorescent protein
592 mutant TSapphire and DsRed variant mOrange to set up a versatile in planta FRET-
593 FLIM assay. Plant physiology. 2008;148(1):51-60. Epub 2008/07/16. doi:
594 10.1104/pp.108.117358. PubMed PMID: 18621983; PubMed Central PMCID:
595 PMCPMC2528103.
596 8. Kredel S, Oswald F, Nienhaus K, Deuschle K, Rocker C, Wolff M, et al. mRuby, a
597 bright monomeric red fluorescent protein for labeling of subcellular structures. PLoS
598 One. 2009;4(2):e4391. Epub 2009/02/06. doi: 10.1371/journal.pone.0004391. PubMed
599 PMID: 19194514; PubMed Central PMCID: PMCPMC2633614.

600 9. Lam AJ, St-Pierre F, Gong Y, Marshall JD, Cranfill PJ, Baird MA, et al. Improving
601 FRET dynamic range with bright green and red fluorescent proteins. Nature methods.
602 2012;9:1005. doi: 10.1038/nmeth.2171
603 https://www.nature.com/articles/nmeth.2171#supplementary-information.
604 10. Bajar BT, Wang ES, Lam AJ, Kim BB, Jacobs CL, Howe ES, et al. Improving
605 brightness and photostability of green and red fluorescent proteins for live cell imaging
606 and FRET reporting. Scientific Reports. 2016;6:20889. doi: 10.1038/srep20889
607 https://www.nature.com/articles/srep20889#supplementary-information.
608 11. Bindels DS, Haarbosch L, van Weeren L, Postma M, Wiese KE, Mastop M, et al.
609 mScarlet: a bright monomeric red fluorescent protein for cellular imaging. Nature
610 methods. 2017;14(1):53-6. Epub 2016/11/22. doi: 10.1038/nmeth.4074. PubMed PMID:
611 27869816.
612 12. Rodriguez EA, Campbell RE, Lin JY, Lin MZ, Miyawaki A, Palmer AE, et al. The
613 Growing and Glowing Toolbox of Fluorescent and Photoactive Proteins. Trends in
614 biochemical sciences. 2017;42(2):111-29. Epub 2016/11/07. doi:
615 10.1016/j.tibs.2016.09.010. PubMed PMID: 27814948; PubMed Central PMCID:
616 PMCPMC5272834.
617 13. Kremers G-J, Gilbert SG, Cranfill PJ, Davidson MW, Piston DW. Fluorescent
618 proteins at a glance. Journal of Cell Science. 2011;124(2):157-60. doi:
619 10.1242/jcs.072744.
620 14. Chudakov DM, Matz MV, Lukyanov S, Lukyanov KA. Fluorescent Proteins and
621 Their Applications in Imaging Living Cells and Tissues. Physiological Reviews.
622 2010;90(3):1103-63. doi: 10.1152/physrev.00038.2009. PubMed PMID: 20664080.
623 15. Lambert TJ. FPbase: a community-editable fluorescent protein database. Nature
624 methods. 2019;16(4):277-8. doi: 10.1038/s41592-019-0352-8.

625 16. Greenwald EC, Mehta S, Zhang J. Genetically Encoded Fluorescent Biosensors
626 Illuminate the Spatiotemporal Regulation of Signaling Networks. Chemical Reviews.
627 2018;118(24):11707-94. doi: 10.1021/acs.chemrev.8b00333.
628 17. Vogel SS, Thaler C, Koushik SV. Fanciful FRET. Science's STKE : signal
629 transduction knowledge environment. 2006;2006(331):re2. Epub 2006/04/20. doi:
630 10.1126/stke.3312006re2. PubMed PMID: 16622184.
631 18. Wall AC, Gius JP, Buglewicz DJ, Banks AB, Kato TA. Oxidative stress and
632 endoreduplication induced by blue light exposure to CHO cells. Mutation research.
633 2019;841:31-5. Epub 2019/05/30. doi: 10.1016/j.mrgentox.2019.05.003. PubMed PMID:
634 31138408.
635 19. Shibuya K, Onodera S, Hori M. Toxic wavelength of blue light changes as insects
636 grow. PLoS One. 2018;13(6):e0199266. Epub 2018/06/20. doi:
637 10.1371/journal.pone.0199266. PubMed PMID: 29920536; PubMed Central PMCID:
638 PMCPMC6007831.
639 20. Arthaut LD, Jourdan N, Mteyrek A, Procopio M, El-Esawi M, d'Harlingue A, et al.
640 Blue-light induced accumulation of reactive oxygen species is a consequence of the
641 Drosophila cryptochrome photocycle. PLoS One. 2017;12(3):e0171836. Epub
642 2017/03/16. doi: 10.1371/journal.pone.0171836. PubMed PMID: 28296892; PubMed
643 Central PMCID: PMCPMC5351967.
644 21. Nakanishi-Ueda T, Majima HJ, Watanabe K, Ueda T, Indo HP, Suenaga S, et al.
645 Blue LED light exposure develops intracellular reactive oxygen species, lipid
646 peroxidation, and subsequent cellular injuries in cultured bovine retinal pigment
647 epithelial cells. Free Radical Research. 2013;47(10):774-80. doi:
648 10.3109/10715762.2013.829570.

649 22. Jou MJ, Jou SB, Guo MJ, Wu HY, Peng TI. Mitochondrial reactive oxygen
650 species generation and calcium increase induced by visible light in astrocytes. Ann N Y
651 Acad Sci. 2004;1011:45-56. Epub 2004/05/06. PubMed PMID: 15126282.
652 23. Siegel AP, Baird MA, Davidson MW, Day RN. Strengths and weaknesses of
653 recently engineered red fluorescent proteins evaluated in live cells using fluorescence
654 correlation spectroscopy. International journal of molecular sciences.
655 2013;14(10):20340-58. Epub 2013/10/17. doi: 10.3390/ijms141020340. PubMed PMID:
656 24129172; PubMed Central PMCID: PMCPMC3821618.
657 24. Shemiakina II, Ermakova GV, Cranfill PJ, Baird MA, Evans RA, Souslova EA, et
658 al. A monomeric red fluorescent protein with low cytotoxicity. Nature communications.
659 2012;3:1204. doi: 10.1038/ncomms2208
660 https://www.nature.com/articles/ncomms2208#supplementary-information.
661 25. Hoffman RM. Chapter eleven - Live Cell Imaging in Live Animals with
662 Fluorescent Proteins. In: Conn PM, editor. Methods in Enzymology. 506: Academic
663 Press; 2012. p. 197-224.
664 26. Campbell RE, Tour O, Palmer AE, Steinbach PA, Baird GS, Zacharias DA, et al.
665 A monomeric red fluorescent protein. Proceedings of the National Academy of
666 Sciences. 2002;99(12):7877-82. doi: 10.1073/pnas.082243699.
667 27. Lin F, Zhang C, Du M, Wang L, Mai Z, Chen T. Superior robustness of ExEm-
668 spFRET to IIem-spFRET method in live-cell FRET measurement. Journal of
669 microscopy. 2018;272(2):145-50. Epub 2018/10/20. doi: 10.1111/jmi.12755. PubMed
670 PMID: 30338530.
671 28. Koushik SV, Chen H, Thaler C, Puhl HL, 3rd, Vogel SS. Cerulean, Venus, and
672 VenusY67C FRET reference standards. Biophys J. 2006;91(12):L99-l101. Epub

673 2006/10/17. doi: 10.1529/biophysj.106.096206. PubMed PMID: 17040988; PubMed
674 Central PMCID: PMCPMC1779932.
675 29. Schindelin J, Arganda-Carreras I, Frise E, Kaynig V, Longair M, Pietzsch T, et al.
676 Fiji: an open-source platform for biological-image analysis. Nature methods.
677 2012;9(7):676-82. Epub 2012/06/30. doi: 10.1038/nmeth.2019. PubMed PMID:
678 22743772; PubMed Central PMCID: PMCPMC3855844.
679 30. Raschka S. MLxtend: Providing machine learning and data science utilities and
680 extensions to Python's scientific computing stack. Journal of Open Source Software.
681 2018;3(24). doi: 10.21105/joss.00638.
682 31. Clavel D, Gotthard G, von Stetten D, De Sanctis D, Pasquier H, Lambert GG, et
683 al. Structural analysis of the bright monomeric yellow-green fluorescent protein
684 mNeonGreen obtained by directed evolution. Acta crystallographica Section D,
685 Structural biology. 2016;72(Pt 12):1298-307. Epub 2016/12/06. doi:
686 10.1107/s2059798316018623. PubMed PMID: 27917830; PubMed Central PMCID:
687 PMCPMC5137226.
688 32. Padilla-Parra S, Auduge N, Lalucque H, Mevel JC, Coppey-Moisan M, Tramier
689 M. Quantitative comparison of different fluorescent protein couples for fast FRET-FLIM
690 acquisition. Biophys J. 2009;97(8):2368-76. Epub 2009/10/22. doi:
691 10.1016/j.bpj.2009.07.044. PubMed PMID: 19843469; PubMed Central PMCID:
692 PMCPMC2764072.
693 33. Molina RS, Tran TM, Campbell RE, Lambert GG, Salih A, Shaner NC, et al.
694 Blue-Shifted Green Fluorescent Protein Homologues Are Brighter than Enhanced
695 Green Fluorescent Protein under Two-Photon Excitation. The Journal of Physical
696 Chemistry Letters. 2017;8(12):2548-54. doi: 10.1021/acs.jpclett.7b00960.

697 34. Mastop M, Bindels DS, Shaner NC, Postma M, Gadella TWJ, Jr., Goedhart J.
698 Characterization of a spectrally diverse set of fluorescent proteins as FRET acceptors
699 for mTurquoise2. Sci Rep. 2017;7(1):11999. Epub 2017/09/22. doi: 10.1038/s41598-
700 017-12212-x. PubMed PMID: 28931898; PubMed Central PMCID: PMCPMC5607329.
701 35. George Abraham B, Sarkisyan KS, Mishin AS, Santala V, Tkachenko NV, Karp
702 M. Fluorescent Protein Based FRET Pairs with Improved Dynamic Range for
703 Fluorescence Lifetime Measurements. PLoS One. 2015;10(8):e0134436. Epub
704 2015/08/04. doi: 10.1371/journal.pone.0134436. PubMed PMID: 26237400; PubMed
705 Central PMCID: PMCPMC4523203.
706 36. Martin KJ, McGhee EJ, Schwarz JP, Drysdale M, Brachmann SM, Stucke V, et
707 al. Accepting from the best donor; analysis of long-lifetime donor fluorescent protein
708 pairings to optimise dynamic FLIM-based FRET experiments. PLoS One.
709 2018;13(1):e0183585. Epub 2018/01/03. doi: 10.1371/journal.pone.0183585. PubMed
710 PMID: 29293509; PubMed Central PMCID: PMCPMC5749721.
711 37. Akerboom J, Carreras Calderón N, Tian L, Wabnig S, Prigge M, Tolö J, et al.
712 Genetically encoded calcium indicators for multi-color neural activity imaging and
713 combination with optogenetics. Frontiers in Molecular Neuroscience. 2013;6(2). doi:
714 10.3389/fnmol.2013.00002.
715

716 # Supplemental Information

717 **S1 Fig. Construct emission scans used for spectral FRET. (A)** Emission scans of several independent
718 transfections of NG-Stop when excited at 470 nm overlaid with the reported emission of pure mNeonGreen. The
719 average of these scans is shown in Fig 2B. Because of the consistency of NG-Stop with the pure mNeonGreen
720 spectrum, the pure mNeonGreen spectrum was used as the donor spectrum for linear unmixing. Acceptor emission
721 scans from several independent transfections of **(B)** NG-Ruby3, **(D)** NG-Scarlet, and **(F)** NG-Cherry achieved by
722 exciting the acceptor directly using 530 and 540 nm light, overlaid with the reported pure spectrum for the red FP in

723 each condition. The average of each condition is shown next to the reported pure spectrum for each acceptor is
724 shown in **(C)**, **(E)**, and **(G)** respectively. Scan of both mScarlet-I and mCherry in the NG-Scarlet and NG-Cherry
725 constructs faithfully replicated the upstroke and peak of purified mScarlet-I and mCherry, with the major difference
726 between the observed and pure protein spectrum being a faster decay of the tail of the spectrum at high wavelengths.
727 In contrast, the scans of mRuby3 in the NG-Ruby3 construct revealed an emission spectrum that was 6 nm shifted
728 from what was reported for purified mRuby3. Due to the differences seen with each of the red acceptor proteins and
729 varying levels of background, custom acceptor emission spectrums were created to serve as the acceptor emission
730 for linear umixing shown in **(C)**, **(E)**, and **(G)** as the black dashed line. The raw traces used to determine the efficiency
731 of **(H)** NG-Ruby3, **(I)** NG-Scarlet, and **(J)** NG-Cherry are shown, corresponding to the efficiency graph in Fig 2F.

732

733 **S2 Fig. Workflow for confocal imaging analysis.** Example workflow demonstrating how confocal images were
734 processed to create intensity slope histograms in Fig 5.

735

736 **S3 Fig. Immunoblot of NG-Stop and NG-Red FP tandem constructs.** 10 µg of total protein derived from cell
737 transiently transfected with the given construct one day post transfection was loaded into a 16% SDS-PAGE gel and
738 mNeonGreen was visualized using an anti-mNeonGreen antibody. NG-Stop has a single band near it's predicted
739 molecular weight of 27kDa. Each of the tandems display two bands, one at the full predicted weight of 54kDA, and
740 one slightly below 50 kDa. Importantly, the NG-Ruby3 construct does not contain a band at a similar weight as the
741 band in the NG-Stop lane, indicating that proteolytic cleavage of the NG-Ruby3 construct does not explain the
742 heterogeneity in cell expressing observed under confocal microscopy.

743

744 **S4 Fig. Example decay curves from the NG-Ruby3 time series. (A)** Example fluorescence decay curves of a
745 single cells expressing NG-Ruby3 2-5 days post transfection (DPT) representative of the average for each condition.
746 The NG-Stop curve and NG-Ruby3 1 DPT curves from Fig 3C are also shown for reference. **(B)** Example
747 fluorescence decay curves from a single cell expressing NG-Ruby3 5 DPT before and after acceptor photobleaching.
748 The NG-Stop curve from Fig 3C is repeated here for reference.

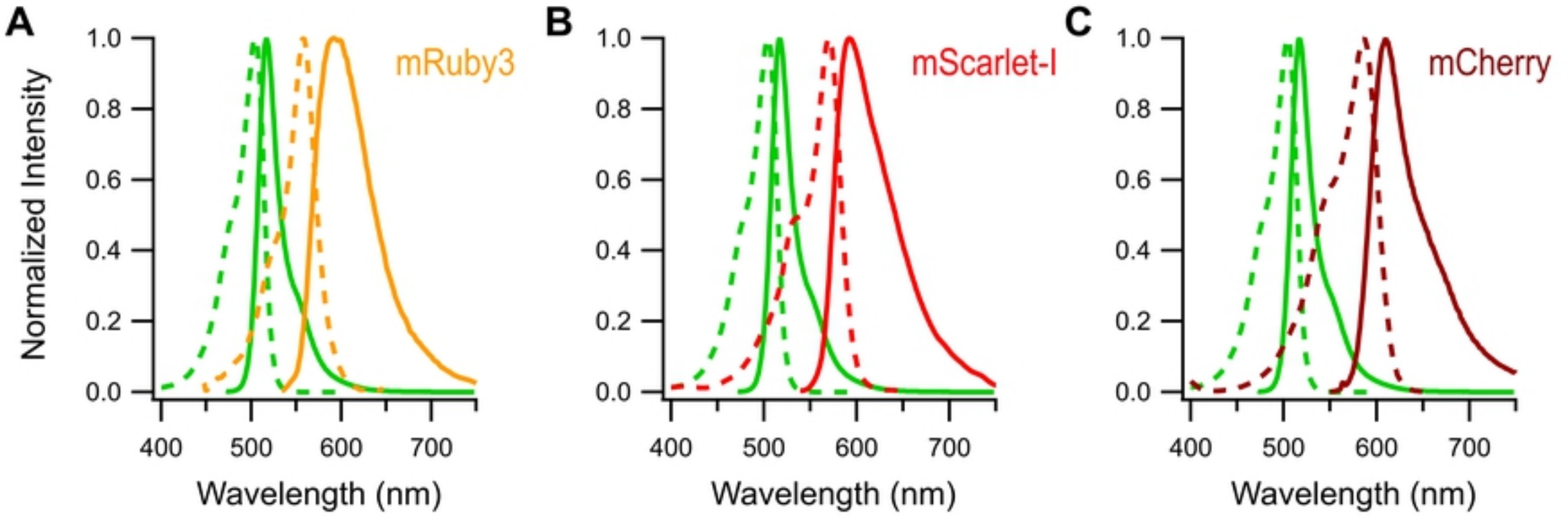
A
B
C
mRuby3
mScarlet-I
mCherry
Normalized Intensity
1.0
0.8
0.6
0.4
0.2
0.0
400
500
600
700
Wavelength (nm)

Figure 1

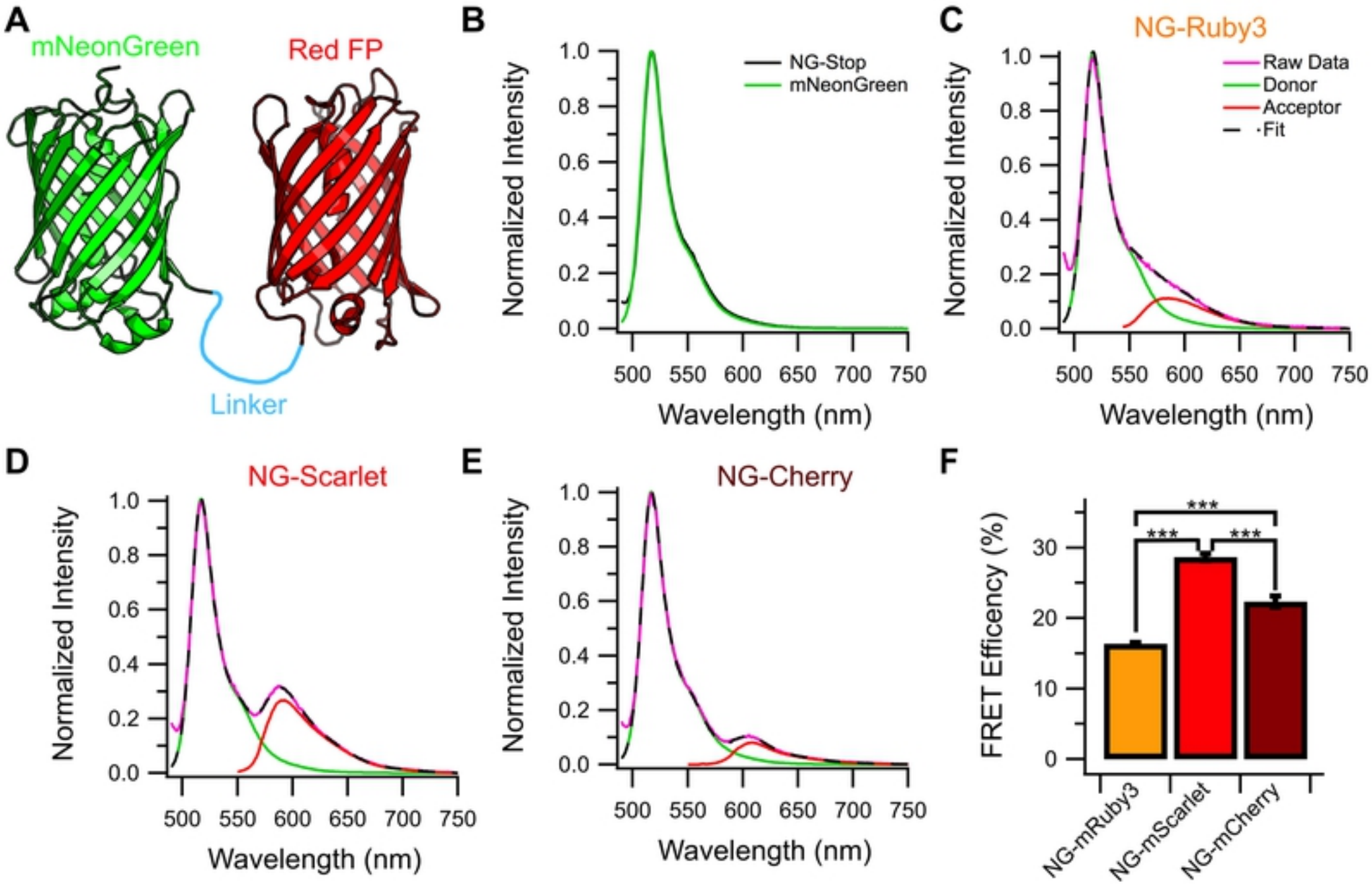
A
mNeonGreen
Red FP
Linker
B
NG-Stop
mNeonGreen
Normalized Intensity
Wavelength (nm)
C
NG-Ruby3
Raw Data
Donor
Acceptor
Fit
Normalized Intensity
Wavelength (nm)
D
NG-Scarlet
Normalized Intensity
Wavelength (nm)
E
NG-Cherry
Normalized Intensity
Wavelength (nm)
F
FRET Efficency (%)
***
***
***
NG-mRuby3
NG-mScarlet
NG-mCherry

Figure 2

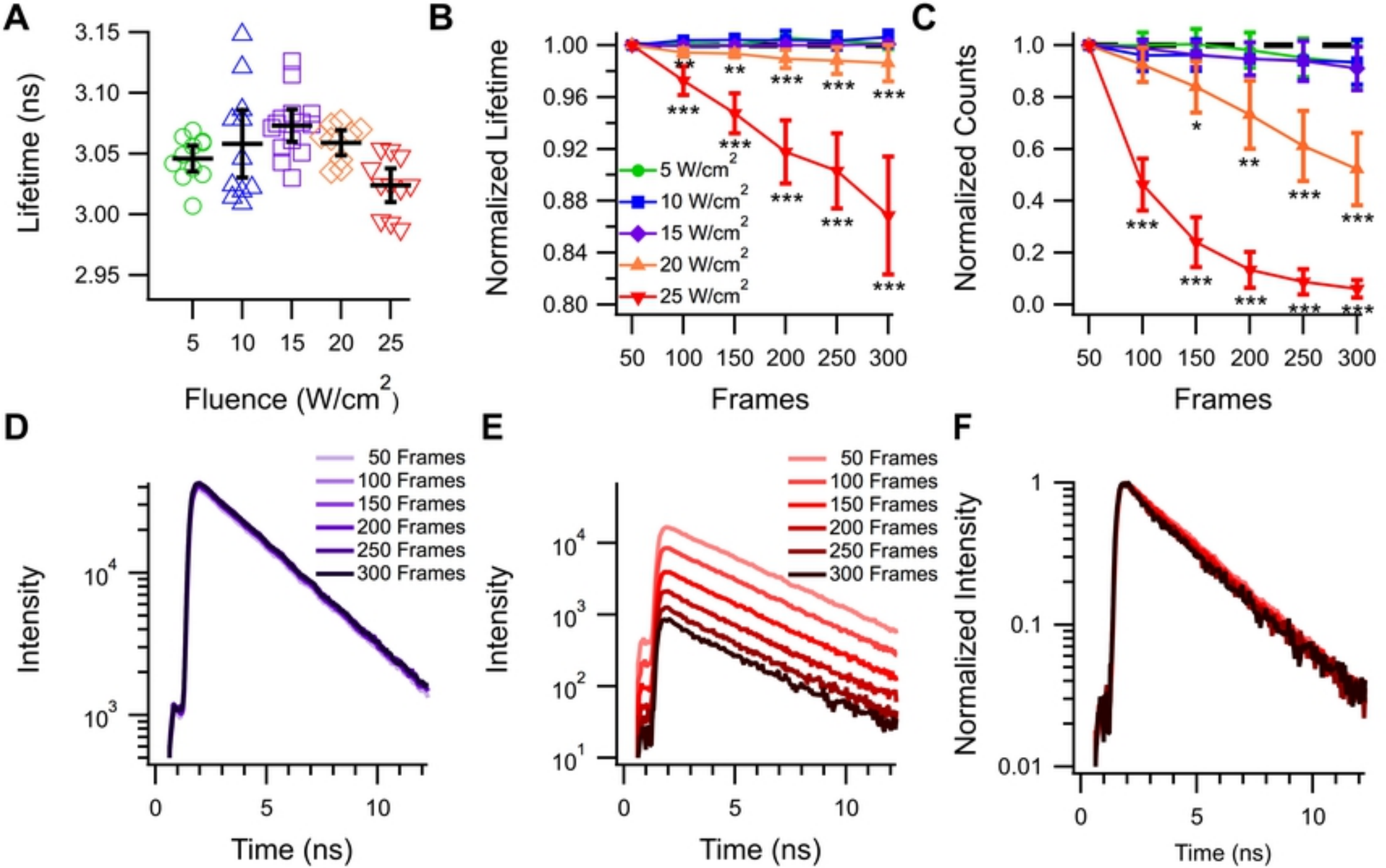
A
Lifetime (ns)
3.15
3.10
3.05
3.00
2.95
5
10
15
20
25
Fluence (W/cm2)
B
Normalized Lifetime
1.00
0.96
0.92
0.88
0.84
0.80
5 W/cm2
10 W/cm2
15 W/cm2
20 W/cm2
25 W/cm2
50
100
150
200
250
300
Frames
C
Normalized Counts
1.0
0.8
0.6
0.4
0.2
0.0
Frames
D
Intensity
50 Frames
100 Frames
150 Frames
200 Frames
250 Frames
300 Frames
Time (ns)
E
Intensity
Time (ns)
F
Normalized Intensity
1
0.1
0.01
Time (ns)

Figure 3

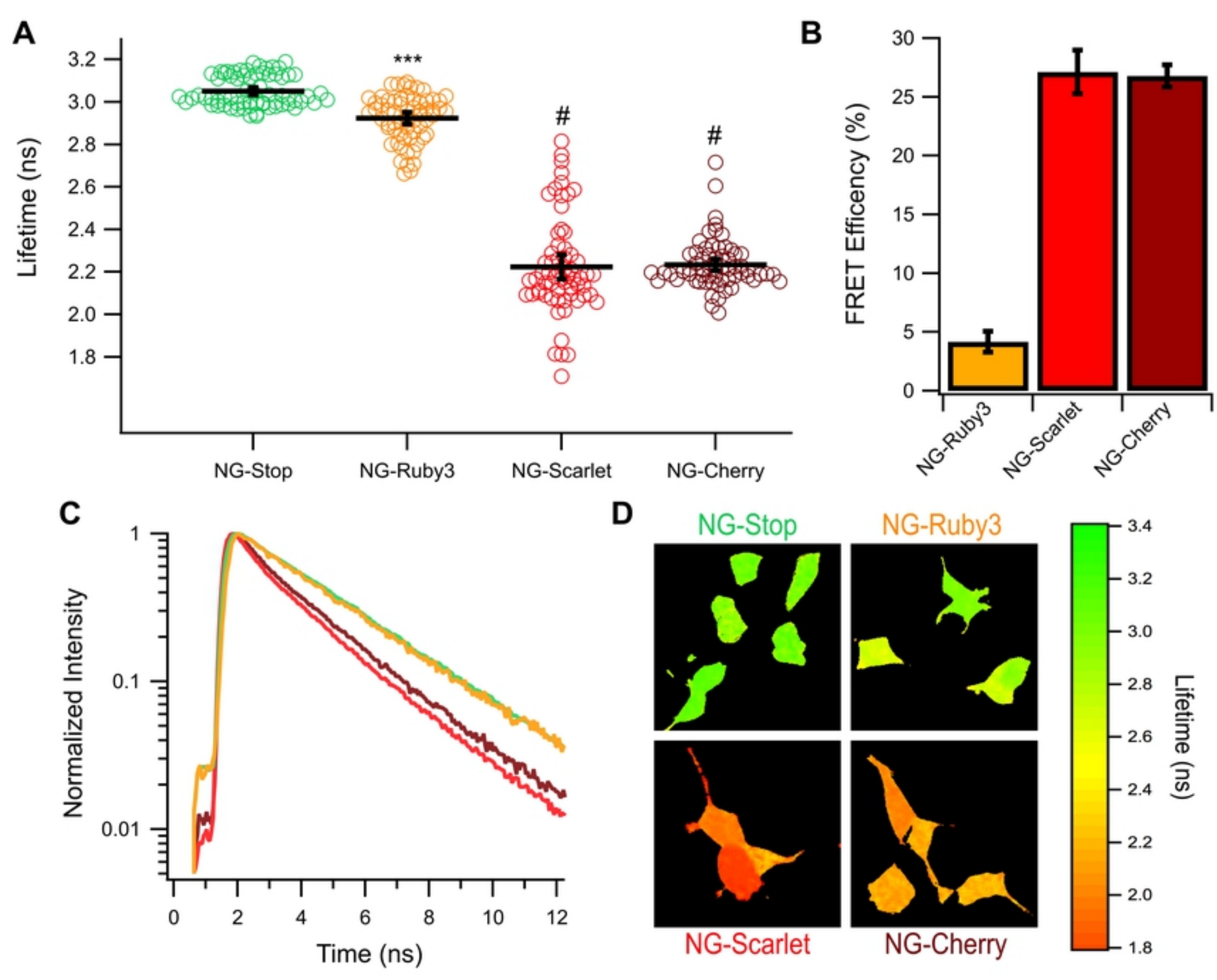
A
Lifetime (ns)
3.2
3.0
2.8
2.6
2.4
2.2
2.0
1.8
***
#
#
NG-Stop
NG-Ruby3
NG-Scarlet
NG-Cherry
B
FRET Efficency (%)
30
25
20
15
10
5
0
NG-Ruby3
NG-Scarlet
NG-Cherry
C
Normalized Intensity
1
0.1
0.01
0
2
4
6
8
10
12
Time (ns)
D
NG-Stop
NG-Ruby3
NG-Scarlet
NG-Cherry
Lifetime (ns)
3.4
3.2
3.0
2.8
2.6
2.4
2.2
2.0
1.8

Figure 4

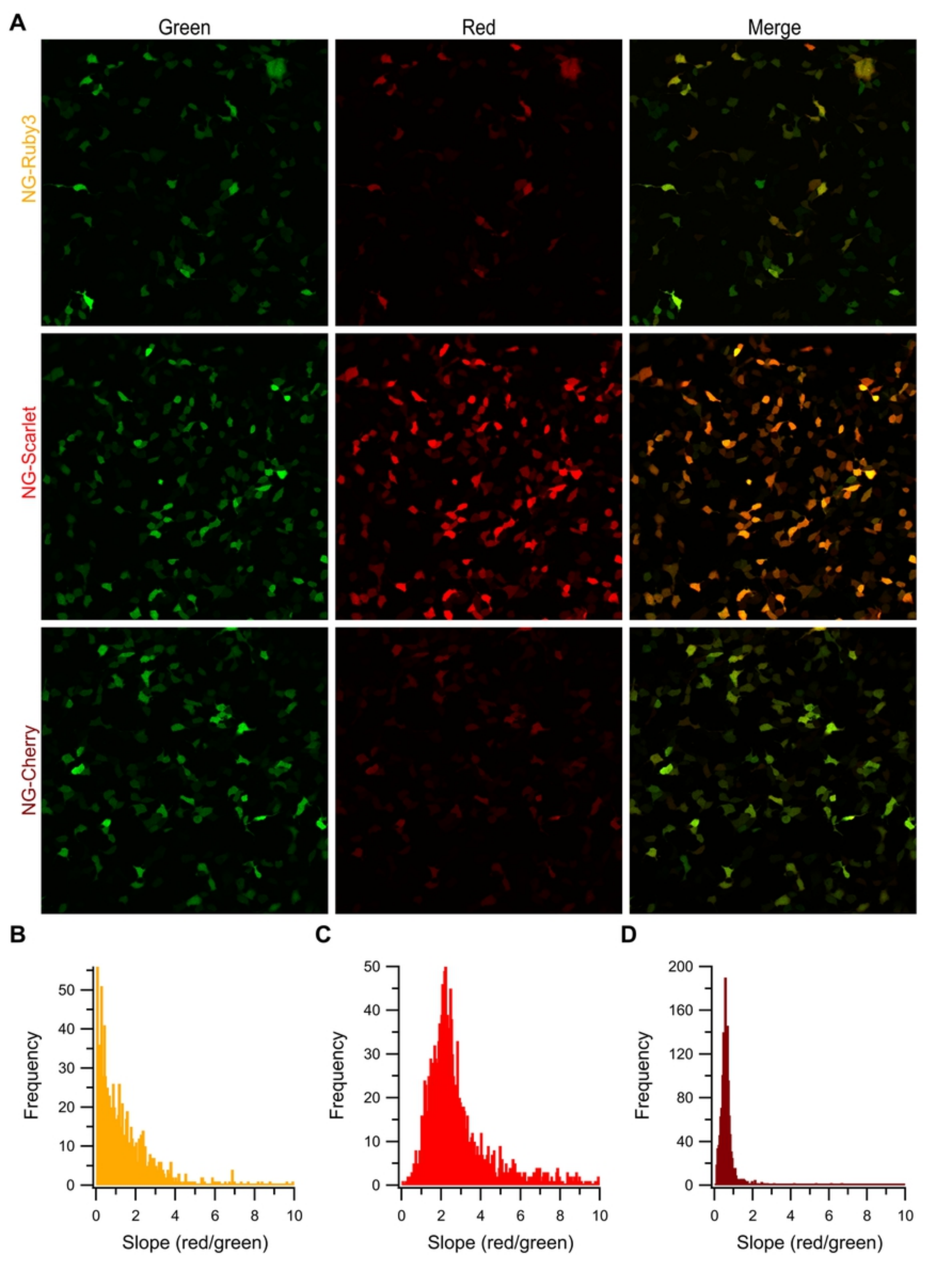
A
Green
Red
Merge
NG-Ruby3
NG-Scarlet
NG-Cherry
B
C
D
Frequency
Slope (red/green)
0
10
20
30
40
50
60
80
120
160
200
2
4
6
8

Figure 5

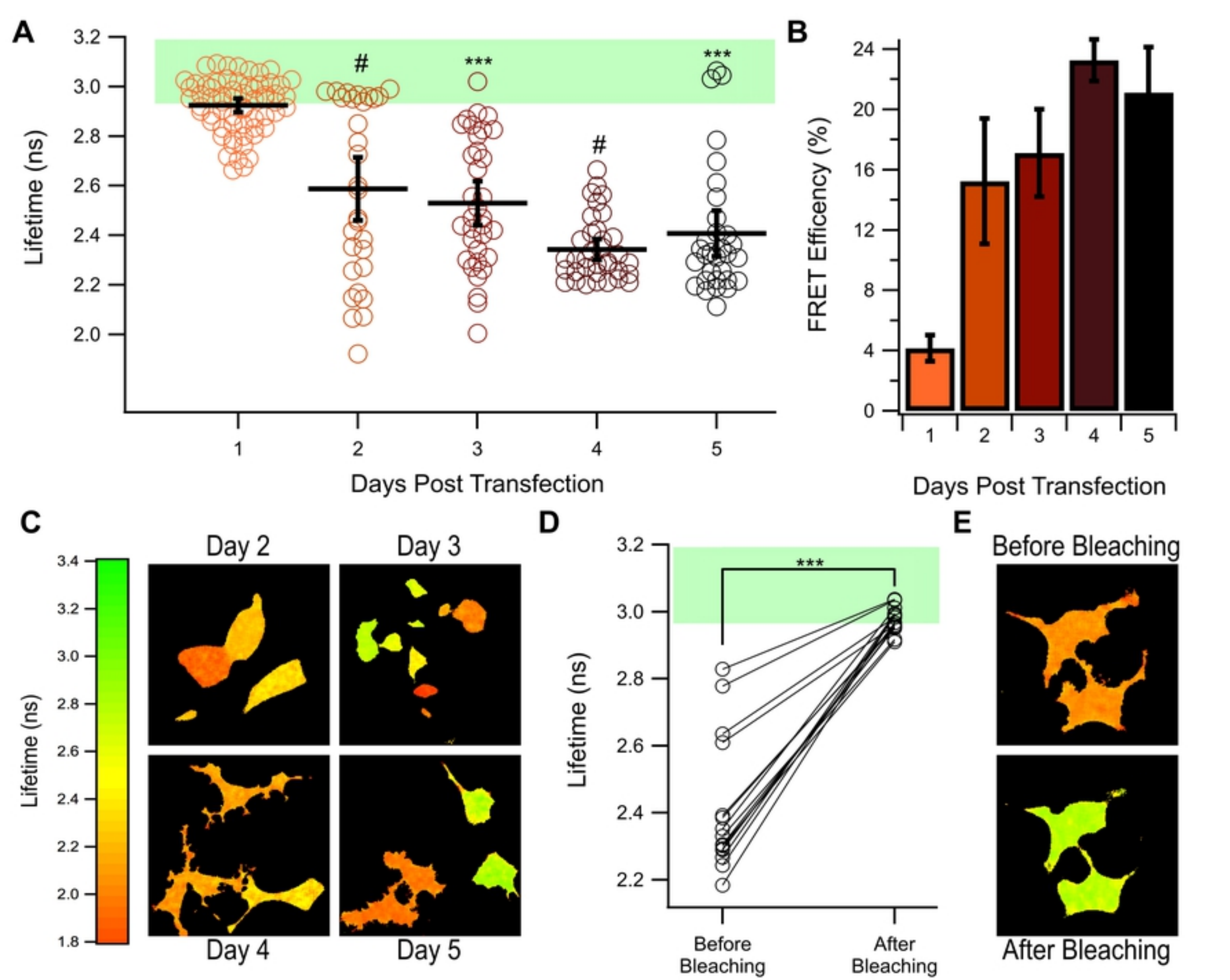
A
Lifetime (ns)
3.2
3.0
2.8
2.6
2.4
2.2
2.0
#
***
#
***
1
2
3
4
5
Days Post Transfection
B
FRET Efficency (%)
24
20
16
12
8
4
0
1
2
3
4
5
Days Post Transfection
C
Day 2
Day 3
Day 4
Day 5
Lifetime (ns)
3.4
3.2
3.0
2.8
2.6
2.4
2.2
2.0
1.8
D
Lifetime (ns)
3.2
3.0
2.8
2.6
2.4
2.2
***
Before Bleaching
After Bleaching
E
Before Bleaching
After Bleaching

Figure 6